J|A|C|S ARTICLES

Published on Web 07/27/2010

Layer-by-Layer Assembly of Three-Dimensional Colloidal Supercrystals with Tunable Plasmonic Properties

Meng-Hsien Lin,[†] Hung-Ying Chen,[‡] and Shangjr Gwo*[,†,‡]

Institute of Nanoengineering and Microsystems and Department of Physics, National Tsing-Hua University, Hsinchu 30013, Taiwan

Received May 8, 2010; E-mail: gwo@phys.nthu.edu.tw

Abstract: We present a simple and efficient method for synthesizing large-area (>1 cm^2), three-dimensional (3D) gold and silver nanoparticle supercrystal films. In this approach, Janus nanoparticle (top face solvent-phobic and bottom face solvent-philic) films with an arbitrary number of close-packed nanoparticle monolayers can be formed using layer-by-layer (LbL) assembly from suspensions of thiolate-passivated gold or silver colloids. Furthermore, we demonstrate that these films can act as true 3D plasmonic crystals with strong transverse (intralayer) and longitudinal (interlayer) near-field coupling. In contrast to conventional polyelectrolyte-mediated LbL assembly processes, this approach allows multiple longitudinal coupling modes with a conspicuous spectral dependence on the layer number. We have found a universal scaling relation between the spectral position of the reflectance dips related to the longitudinal modes and the layer number. This relation can be understood in terms of the presence of a plasmonic Fabry−Pérot nanocavity along the longitudinal direction that allows the formation of standing plasmon waves under plasmon resonance conditions. The realization of 3D plasmonic coupling enables broadband tuning of the collective plasmon response over a wide spectral range (visible and near-IR) and provides a pathway to designer plasmonic metamaterials.

Introduction

One of the outstanding challenges in the emerging fields of plasmonics[1−3] and metamaterials[4−6] is large-scale self-assembly[7−12] of nanomaterials into macroscopic supercrystals that exhibit collective properties. In particular, it has been anticipated that three-dimensional (3D) noble-metal nanostructure arrays with strong and tunable plasmonic response could allow the creation of novel optical materials.[5,6] Colloidal gold and silver nanoparticles (AuNPs and AgNPs, respectively) are attractive candidates as nanoscale plasmonic building blocks because of their size monodispersity, shape controllability, facile surface functionalization, and unique optical properties in the visible-light region. Spherical AuNPs and AgNPs dispersed in solutions show characteristic red and yellow colors, respectively, when their sizes are in the quasistatic size regime (5−50 nm). This well-known phenomenon has its physical origin in localized plasmon resonance (LPR) of conduction electrons in AuNPs and AgNPs with the incident optical field, and the LPR peak wavelength strongly depends on the particle size and shape as well as on the surrounding dielectric environment. In the past few years, the LPR properties have been utilized in chemical and biological sensing applications. Recently, considerable attention has been directed to studies of near-field-coupled noble-metal nanoparticle systems because of their tunable plasmonic properties, which are very desirable for a variety of applications. Among these systems, the coupling effects of plasmonic dimers consisting of two nanoparticles placed next to each other within the near-field range have been widely studied.[13−17] For more complex systems, it has become clear that collective plasmon resonance (CPR) in coupled colloidal AuNP or AgNP arrays can manifest itself through plasmonic crystal effects.[18−20] In a recent work, we have shown that the CPR modes can be

[†] Institute of Nanoengineering and Microsystems.
[‡] Department of Physics.

(1) Barnes, W. L.; Dereux, A.; Ebbesen, T. W. *Nature* **2003**, *424*, 824–830.
(2) Maier, S. A.; Atwater, H. A. *J. Appl. Phys.* **2005**, *98*, 011101.
(3) Wang, H.; Brandl, D. W.; Nordlander, P.; Halas, N. J. *Acc. Chem. Res.* **2007**, *40*, 53–62.
(4) Smith, D. R.; Pendry, J. B.; Wiltshire, M. C. K. *Science* **2004**, *305*, 788–792.
(5) Valentine, J.; Zhang, S.; Zentgraf, T.; Ulin-Avila, E.; Genov, D. A.; Bartal, G.; Zhang, X. *Nature* **2008**, *455*, 376–379.
(6) Liu, N.; Guo, H. C.; Fu, L. W.; Kaiser, S.; Schweizer, H.; Giessen, H. *Nat. Mater.* **2008**, *7*, 31–37.
(7) Collier, C. P.; Saykally, R. J.; Shiang, J. J.; Henrichs, S. E.; Heath, J. R. *Science* **1997**, *277*, 1978–1981.
(8) Murray, C. B.; Kagan, C. R.; Bawendi, M. G. *Annu. Rev. Mater. Sci.* **2000**, *30*, 545–610.
(9) Whitesides, G. M.; Grzybowski, B. *Science* **2002**, *295*, 2418–2421.
(10) Wong, S.; Kitaev, V.; Ozin, G. A. *J. Am. Chem. Soc.* **2003**, *125*, 15589–15598.
(11) Nakanishi, H.; Bishop, K. J. M.; Kowalczyk, B.; Nitzan, A.; Weiss, E. A.; Tretiakov, K. V.; Apodaca, M. M.; Klajn, R.; Stoddart, J. F.; Grzybowski, B. A. *Nature* **2009**, *460*, 371–375.
(12) Baker, J. L.; Widmer-Cooper, A.; Toney, M. F.; Geissler, P. L.; Alivisatos, A. P. *Nano Lett.* **2010**, *10*, 195–201.
(13) Prodan, E.; Radloff, C.; Halas, N. J.; Nordlander, P. *Science* **2003**, *302*, 419–422.
(14) Su, K.-H.; Wei, Q.-H.; Zhang, X.; Mock, J. J.; Smith, D. R.; Schultz, S. *Nano Lett.* **2003**, *3*, 1087–1090.
(15) Nordlander, P.; Oubre, C.; Prodan, E.; Li, K.; Stockman, M. I. *Nano Lett.* **2004**, *4*, 899–903.
(16) Jain, P. K.; Huang, W.; El-Sayed, M. A. *Nano Lett.* **2007**, *7*, 2080–2088.
(17) Yang, S.-C.; Kobori, H.; He, C.-L.; Lin, M.-H.; Chen, H.-Y.; Li, C.; Kanehara, M.; Teranishi, T.; Gwo, S. *Nano Lett.* **2010**, *10*, 632–637.

generated in two-dimensional (2D) self-assembled AuNP superlattices via near-field coupling between neighboring nanoparticles in close-packed superlattices.[19] It has also been confirmed that the CPR peak position can be sensitively tuned by varying the interparticle gap distance. Moreover, Tao et al. have demonstrated that AgNPs can be used as building blocks to construct 3D plasmonic crystals.[20]

However, questions remain about the practicality of self-assembly techniques for fabricating colloidal plasmonic crystals. For example, it is important to demonstrate the feasibility of depositing a single layer of highly ordered nanoparticles over a wafer-scale substrate (to date, the largest 3D nanoparticle crystals grown by self-assembly techniques have been limited to submillimeter dimensions).[21] Furthermore, it would be more controllable to deposit nanoparticle supercrystals in a layer-by-layer (LbL) fashion,[22−24] similar to the molecular-beam epitaxy technique used for fabricating semiconductor devices. If these capabilities can be realized, construction of 3D plasmonic metamaterials with engineerable plasmonic properties would become more practical. Here we report a simple and efficient bottom-up assembly method for achieving such goals. The experimental technique can be applied to deposit close-packed, multilayered nanoparticle films over large-area solid substrates.

Experimental Section

In Figure 1, we show that this method involves two key steps. First, oversaturation conditions of the octadecanethiolate-passivated nanoparticle solution in toluene were generated with a controlled amount of surfactant in order to form a phase-segregated nanoparticle "liquid" floating on top of the solution. Subsequently, nanoparticle monolayers were transferred to any chosen substrate [quartz, indium tin oxide (ITO), silicon, or gold] consecutively by dipping the substrate and pulling it out perpendicular to the liquid surface (dip coating). In comparison with the Langmuir−Blodgett technique, one distinct advantage is that the present approach does not require spreading and compression of the nanoparticle monolayers on the liquid surface (because of self-replenishment from the oversaturated nanoparticle solution). In addition, the assembly kinetics is very fast at high temperatures, on the order of seconds for one full monolayer (ML) coverage onto a 2 cm × 2 cm substrate area. At room temperature, the withdrawal rate for nanoparticle dip coating is ∼30 s/cm, while at high temperature (70 °C), the withdrawal rate can be as high as 2−5 s/cm.

It is important to note that without further surface-ligand modification, only a self-limiting nanoparticle monolayer can be formed. Therefore, stacking of more nanoparticle monolayers would require that the exposed sides of the nanoparticles be converted to solvent-phobic. However, as-synthesized nanoparticles are typically symmetric in surface-ligand structure, allowing only the formation of a single monolayer. Therefore, in order to construct multilayered structures, it is essential to create monolayers of Janus nanoparticles (particles that simultaneously display two distinctly different surface properties[25−34]). We recently introduced a plasma-based surface-modification technique that is suitable for large-scale, solvent-free synthesis of Janus nanoparticle arrays.[35] Through the use of this technique, which is scalable to almost any substrate size, the exposed methyl groups of thiolate-stabilized nanoparticles on the surface can be converted into oxidized moieties (Figure 1a) that are solvent-phobic in toluene. This unique surface property makes the nanoparticle monolayer insoluble in the solvent during subsequent dipping into the nanoparticle solution, allowing for deposition of additional monolayers in an epitaxial growth manner. As shown by the field-emission scanning electron microscopy (FE-SEM) micrograph of the first nanoparticle monolayer (after plasma modification; Figure 1a), the long-range ordering of the first nanoparticle monolayer enables the formation of an epitaxial template for subsequent deposition.

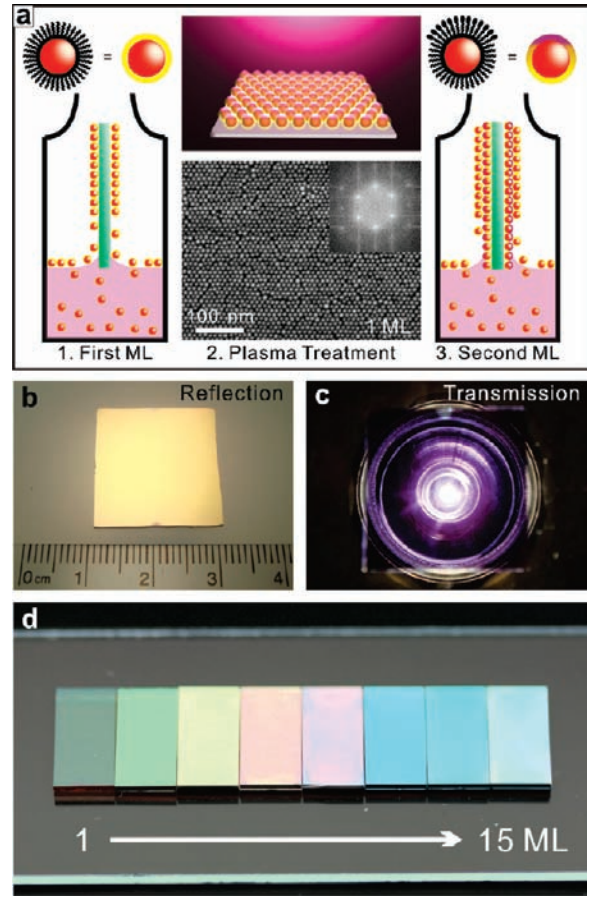

Figure 1. Rainbow plasmonic crystals assembled from gold and silver nanoparticles. (a) Schematic illustration of the plasma-assisted LbL assembly process. The FE-SEM image obtained from the first monolayer of AuNPs after plasma treatment indicates that a long-range close-packed nanoparticle superlattice can be formed by using this technique. The in-plane lattice constant obtained by fast Fourier transform analysis (from an imaging area of 500 nm × 500 nm) is ∼9 nm, and the FE-SEM-measured core diameter of gold nanoparticles is ∼6 nm. The layer-forming process can be repeated for arbitrary times to form multilayered films. (b, c) Plasmonic response of a large-area (2 cm × 2 cm), highly uniform 10 ML AuNP film on quartz, demonstrating the effects of collective plasmonic resonance. The reflection photograph shows that the plasmonic resonance peak (568 nm) is at greenish-yellow, which makes the AuNP film exhibit a hue similar to that of a sputtered gold film. In contrast, the transmission photograph through the film (illuminated by a halogen light source in combination with a flashlight parabolic reflector) shows that this film has a brilliant purple color, which is drastically different from the original ruby-red color of AuNPs dispersed in toluene. (d) Optical reflection from AgNP (∼6 nm diameter) films (∼0.5 cm × 1 cm) with thicknesses of 1, 3, 5, 7, 9, 11, 13, and 15 ML positioned side-by-side. The rainbow-colored photographs result from the combined effect of two plasmonic resonance bands [one constant peak at 468 nm and another one that sensitively depends on the layer number (see Figure 4b)].

(18) Tao, A.; Sinsermsuksakul, P.; Yang, P. *Nat. Nanotechnol.* **2007**, *2*, 435–440.
(19) Chen, C.-F.; Tzeng, S.-D.; Chen, H.-Y.; Lin, K.-J.; Gwo, S. *J. Am. Chem. Soc.* **2008**, *130*, 824–826.
(20) Tao, A. R.; Ceperley, D. P.; Sinsermsuksakul, P.; Neureuther, A. R.; Yang, P. *Nano Lett.* **2008**, *8*, 4033–4038.
(21) Talapin, D. V. *ACS Nano* **2008**, *2*, 1097–1100.
(22) Kotov, N. A.; Dékány, I.; Fendler, J. H. *J. Phys. Chem.* **1995**, *99*, 13065–13069.
(23) Schmitt, J.; Decher, G.; Dressick, W. J.; Brandow, S. L.; Geer, R. E.; Shashidhar, R.; Calvert, J. M. *Adv. Mater.* **1997**, *9*, 61–65.
(24) Brust, M.; Bethell, D.; Kiely, C. J.; Schiffrin, D. J. *Langmuir* **1998**, *14*, 5425–5429.

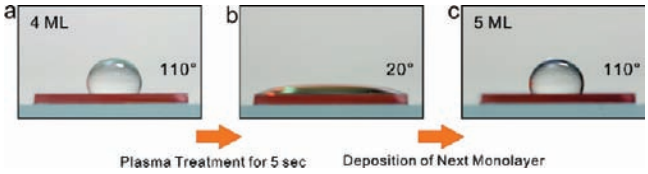

Figure 2. Contact angle measurements on an octadecanethiolate-passivated AgNP supercrystal film deposited on an ITO-coated silica substrate (1 cm width) (a) before and (b) after air-plasma treatment. The supercrystal surface changes from hydrophobic (110°) to hydrophilic (20°) after air-plasma treatment for 5 s. The volume of water droplets is ~100 μL, and the air plasma is generated with the conditions of 7 W (RF power) and 0.3 Torr (pressure of backfilled air). (c) The contact angle recovers to 110° after deposition of an additional AgNP monolayer. Using X-ray photoelectron spectroscopy, we previously showed that the low-power air-plasma treatment can result in oxidation of surface methyl groups.[35]

Combining these two steps (i.e., repetitive dip coating and plasma modification) allows an arbitrary number (up to tens) of nanoparticle monolayers to be efficiently deposited on any chosen substrates with a 3D close-packed structure. Panels b and c of Figure 1 exhibit the collective plasmonic properties of a closed-packed AuNP film (10 ML, deposited on quartz) in the visible-light region. The optical reflectance and transmittance spectra show that the CPR band resulting from intralayer plasmonic coupling (i.e., transverse mode, T-mode) is at ~568 nm. This coupling effect results in the greenish-yellow color in the reflection photograph (Figure 1b). Also, the spectral response explains the origin of the purple color shown in the transmission photograph (Figure 1c). Because the plasmon band is at a longer wavelength than that of dispersed AuNPs in toluene, the AuNP film transmits more blue and less red light, and the transmission of similar amounts of red and blue light causes the observation of a purple color. Detailed spectroscopic measurements showed that there are additional plasmon bands (longitudinal modes, L-modes) in the near-IR region that originate from the effects of interlayer plasmonic coupling. In contrast to the constant T-mode resonance, the reflectance resonant peaks due to the L-modes critically depend on the number of nanoparticle layers in the films. In the case of AgNP films (Figure 1d), the T-mode resonance is at ~468 nm (blue), and the combination of the T-mode and LbL-varied L-mode reflection peaks render the appearance of spectacular rainbow-colored films over the full visible range.

In this work, the air-plasma-based surface-modification method is the key step that allows for the successive formation of close-packed Janus nanoparticle monolayers. To demonstrate this effective surface-modification technique, we performed contact angle measurements for a 4 ML nanoparticle film before and after plasma treatment. As shown in Figure 2, the hydrophobic surface of the 4 ML nanoparticle film can be turned into a hydrophilic surface by a short exposure (5 s) to air plasma. After deposition of an additional nanoparticle monolayer, the film surface recovers to a hydrophobic one, and this process can be repeated many times. According to our previous study, this surface-modification mechanism originates from plasma-induced oxidation of surface methyl groups.[35]

Results and Discussion

Figure 3a,b shows FE-SEM micrographs obtained from the cleaved face of a 10 ML AuNP film deposited on a silicon substrate. The high-resolution micrograph shown in Figure 3b indicates that deposited AuNPs are close-packed in the stacking direction. In Figure S2 in the Supporting Information, we present results of synchrotron X-ray measurements [specular X-ray reflectivity (SXR) and grazing-incidence small-angle X-ray scattering (GISAXS), respectively] that demonstrate both vertical and in-plane long-range supercrystal ordering. Long-range ordering is more suitable for study by X-ray diffraction methods because electron microscopy can access the material properties only on microscopic scales. In comparison, we have found that the X-ray measurement results are in agreement with the fast Fourier transform analysis of the high-resolution SEM superlattice images as well as the average interlayer spacing determined by cross-sectional SEM on a cleaved sample facet.

As demonstrated in Figure 3, this multilayer technique can be applied to the deposition of nanoparticle films having thicknesses of up to 30 ML. Because of the close-packed structure, both transverse and longitudinal near-field plasmonic coupling effects are very strong, allowing the unique opportunity to measure the CPR properties of the 3D plasmonic crystals in these films, especially those originating from the interlayer coupling. Conventional LbL electrostatic self-assembly is a simple yet elegant way to deposit macroscopic, multilayered nanoparticle films onto surfaces functionalized with oppositely charged (e.g., polyelectrolyte) or chemically conjugated (e.g., dithiol) cross-linkers.[22−24] However, the use of cross-linkers drastically reduces the mobility of the individual nanoparticles and hinders the formation of well-ordered superlattices. Therefore, both close packing and long-range ordering are not feasible using these approaches, as evidenced in the related microscopic studies. Moreover, interlayer plasmonic coupling, which is important for the realization of 3D plasmonic metamaterials, is generally nonexistent in these multilayer systems. Here we have overcome these problems by creating layers of monolayers of Janus nanoparticles, making the use of cross-linkers unnecessary.

The 3D CPR characteristics of the nanoparticle films can be clearly observed in the LbL-measured reflectance and absorbance (transmittance) spectra (Figure 4 and Figure S4 in the Supporting Information, respectively). In Figure 4a, the reflectance spectra show the presence of a CPR peak in the T-mode spectral region of the AuNP films. At lower layer numbers, substrate and semitransparency effects are significant, and the reflectance peak positions do not exactly match those of the absorbance spectra (yellow circles). As the layer number is increased to larger than 10 ML, the reflectance peak stabilizes at a fixed spectral position (568 nm) and matches well with the T-mode position in the corresponding absorbance spectra, in agreement with the expected "bulk"-like behavior in this thickness regime. Moreover, clear reflectance dips (marked by order number $m = 1$) start to appear, and they are very different from that measured from a sputtered gold film with a flat, featureless response (a reference spectrum is also shown in Figure 4a). These $m = 1$ reflectance dips shift continuously to longer wavelengths with increasing layer number and move out of the spectroscopic detection range for layer numbers larger than 20. In the subsequent spectra, it is clear that these reflectance dips indicate the onset of L-modes, which originate

(25) de Gennes, P. G. *Rev. Mod. Phys.* **1992**, *64*, 645–648.
(26) Teranishi, T.; Inoue, Y.; Nakaya, M.; Oumi, Y.; Sano, T. *J. Am. Chem. Soc.* **2004**, *126*, 9914–9915.
(27) Perro, A.; Reculusa, S.; Ravaine, S.; Bourgeat-Lami, E.; Duguet, E. *J. Mater. Chem.* **2005**, *15*, 3745–3760.
(28) Roh, K.-H.; Martin, D. C.; Lahann, J. *Nat. Mater.* **2005**, *4*, 759–763.
(29) Hong, L.; Cacciuto, A.; Luijten, E.; Granick, S. *Nano Lett.* **2006**, *6*, 2510–2514.
(30) Glotzer, S. C.; Solomon, M. J. *Nat. Mater.* **2007**, *6*, 557–562.
(31) Walther, A.; Müller, A. H. E. *Soft Matter* **2008**, *4*, 663–668.
(32) Granick, S.; Jiang, S.; Chen, Q. *Phys. Today* **2009**, *62*, 68–69.
(33) Ohnuma, A.; Cho, E. C.; Camargo, P. H. C.; Au, L.; Ohtani, B.; Xia, Y. N. *J. Am. Chem. Soc.* **2009**, *131*, 1352–1353.
(34) McConnell, M. D.; Kraeutler, M. J.; Yang, S.; Composto, R. J. *Nano Lett.* **2010**, *10*, 603–609.
(35) Lin, M.-H.; Chen, C.-F.; Shiu, H.-W.; Chen, C.-H.; Gwo, S. *J. Am. Chem. Soc.* **2009**, *131*, 10984–10991.

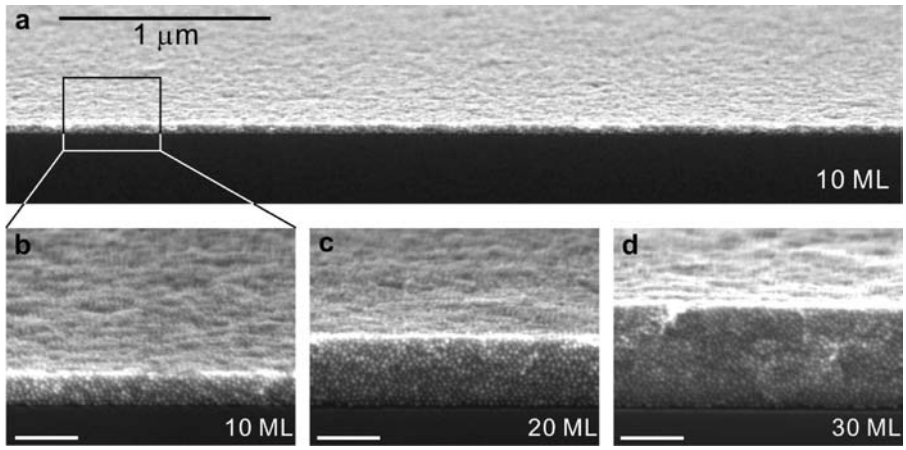

Figure 3. FE-SEM micrographs of AuNP supercrystal films. (a) Large-area and (b) high-resolution cross-sectional SEM micrographs of a 10 ML AuNP film deposited on a Si substrate (imaged on the cleaved face). (c, d) Cross-sectional SEM micrographs of 20 and 30 ML AuNP films deposited on Si substrates. Individual AuNPs (~6 nm core diameter) in the films are clearly resolved in the high-resolution SEM micrographs. The cross-sectional micrographs confirm the close-packed stacking during the LbL assembly process of multilayered structures. We have demonstrated that at least a few tens of ML of AuNPs or AgNPs can be successively deposited on a variety of substrates without significant film cracking. The scale bars in the high-resolution micrographs indicate 100 nm.

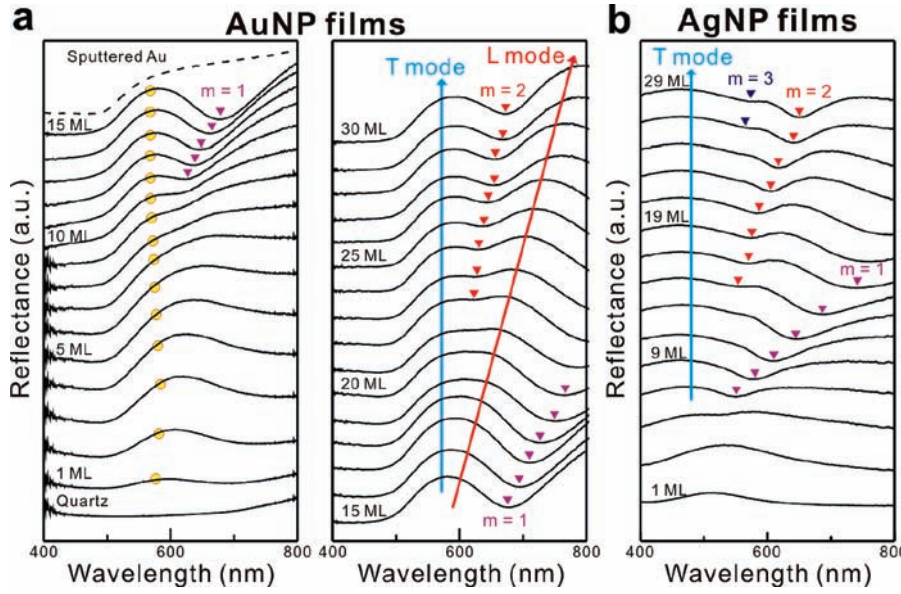

Figure 4. LbL-measured reflectance spectra of AuNP and AgNP films. (a) Reflectance measurements at normal incidence for a sequentially deposited AuNP film on a quartz substrate. The yellow circles denote the peak positions of absorbance spectra from 1 to 15 ML, which were derived from transmittance measurements (Figure S4 in the Supporting Information). The reflectance spectra have been vertically shifted for clarity. After 10 ML, the reflectance peak of the T-mode stabilizes at a constant spectral position (568 nm). Both transverse (T-mode) and longitudinal (L-mode) plasmonic modes are clearly discernible from 15 to 30 ML. (b) Reflectance measurements at normal incidence for a sequentially deposited AgNP film on a quartz substrate (only odd-layer-number spectra are shown). The reflectance peak of the T-mode is at 468 nm. Reflection photographs of AgNP films illuminated with white light (Figure 1d) exhibit layer-number-dependent colors due to the mixing of reflected light from T- and L-mode resonances.

from the interlayer CPR and shift into the near-IR region of the spectrum with increasing layer number. For the case of AgNP films with the T-mode reflectance peak at 468 nm (Figure 4b), the L-mode reflectance peaks are in the visible, and the AgNP films dramatically change the reflection color even with addition of a single monolayer.

In Figure 4, we can also clearly identify the higher order L-modes ($m = 2$ and $m = 3$ reflectance dips), which split off from the T-mode peak and move gradually toward longer wavelengths. In view of the high opacity of nanoparticle films with large numbers of layers, the observation of intense L-modes and their dependence on the layer number ("bulk" properties) in the reflectance spectra indicates the importance of interlayer plasmonic coupling. In Figure 5, we show that for both the AuNP and AgNP films, any lowest-order ($m = 1$) resonant dips for the N-layer films can repeatedly appear when the layer number is mN for the higher order ($m \neq 1$) reflectance dips. This universal scaling relation can be explained in terms of standing plasmon waves in one-dimensional (1D) plasmonic cavities (Au and Ag nanowires[36−40] and nanofabricated Au−SiO_2−Au thin-film waveguides[41]). In the case of discrete systems (N = integer), at the m^{th} resonance in a plasmonic cavity with length L, the cavity resonance conditions are

$$L = Na = \frac{m\lambda_p}{2} \quad (1)$$

where L is the cavity length, N is the number of layers, a is the interlayer spacing, $m = 1, 2, 3, \ldots$ is the resonance order number, and λ_p is the plasmon wavelength. Thus, the corresponding wave

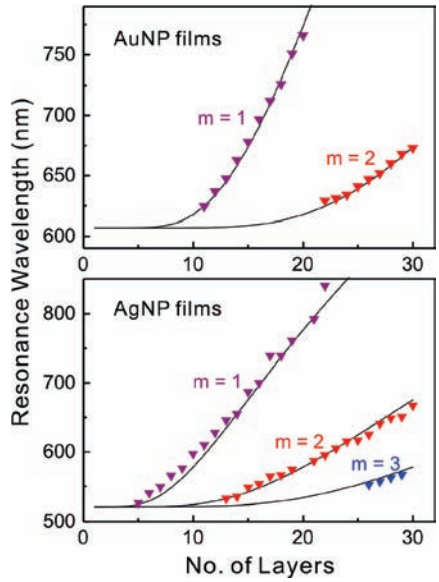

Figure 5. Universal scaling relation of L-modes. Free-space wavelengths of reflectance dips in the LbL-measured spectra (shown in Figure 3) of AuNP and AgNP films are plotted as functions of the layer number (N) and the resonance order number ($m = 1, 2, 3$). As shown in this figure, any lowest-order ($m = 1$) resonant dips for the N-layer films can repeatedly appear when the layer number is mN for the higher-order ($m > 1$) resonances. This can be understood in terms of the presence of a plasmonic Fabry−Pérot nanocavity along the longitudinal direction. The solid lines represent fits to the spectral positions of the reflectance dips using the universal scaling relation given by eq 2: $\lambda_N = \lambda_s + A\lambda_s \exp(-\beta m/N)$, where λ_N is the resonance wavelength of N coupling layers, λ_s is the resonance wavelength of a single monolayer (i.e., the T-mode wavelength), and A and β are parameters related to the asymptotic shift and the interlayer coupling range, respectively.

vector of the propagating plasmon, k_p, can be expressed using eq 1 as $k_p = 2\pi/\lambda_p = m\pi/Na$. On the basis of the plasmon wave dispersion relation,[36,41] the resonant photon energy hc/λ, in which h is Planck's constant, c is the speed of light in free space, and λ is the free-space wavelength, is a function of k_p. Since k_p is proportional to m/N, we can observe the periodic occurrence of any resonant free-space wavelength (λ) at lowest order with proportionally increased layer numbers at higher resonance order.

A recent theoretical study by Harris et al.[42] showed that the longitudinal plasmonic resonance of 1D near-field-coupled gold nanoparticle chain is red-shifted (relative to the resonance of an isolated nanoparticle) with increasing number of nanoparticles in the chain for a fixed interparticle gap. Similar to the behavior of the shift of plasmon resonances in plasmonic dimers,[16] it has also been found that an exponential relation can be used to quantitatively determine the resonance peak shift, which can reach an asymptotic value at increasingly long chain length (large N). We confirmed that the chain model considered in ref 42 can also be applied in our case. By incorporating the scaling relation described above into the peak-shift formula, we obtained the following equation to describe the shift ratio of the resonant reflectance dips:

$$\Delta\lambda_N = \frac{\lambda_N - \lambda_s}{\lambda_s} = A \exp\left(-\beta\frac{m}{N}\right) \qquad (2)$$

where λ_N is the m^{th}-order resonance wavelength of N coupling layers, λ_s is the resonance wavelength of single monolayer (i.e., the T-mode wavelength), A is the asymptotic value, and β is the characteristic interlayer coupling range. Both A and β depend on the detailed plasmonic crystal conditions, such as particle size, composition, interparticle gap, substrate, and so on. The fitting results obtained using this universal scaling relation match with the experimental data very well (Figure 5); the characteristic interlayer coupling ranges (β) are 55 and 30 and the single-monolayer resonance wavelengths (λ_s) are 607 and 520 nm for the AuNP and AgNP films, respectively. As expected, the fitted values of λ_s are very close to the measured T-mode spectral positions for the first monolayer of AuNPs (600 nm) and AgNPs (517 nm) (see Figure 4). The fitted asymptotic constants A are 4.3 and 2.2 for AuNP and AgNP films, respectively. Therefore, the resonance L-mode wavelength in free space could be tuned well into the near-IR region (~3.2 μm for AuNP films and ~1.7 μm for AgNP films). In comparison with the situation for near-field-coupled particle chains, the values of A and β for the film cases are much larger because of the very strong plasmonic interactions in the interlayer coupling geometry.

Conclusions

Although only gold and silver colloids are demonstrated here as building blocks for rationally designed plasmonic metamaterials, the present approach could be extended to other nanomaterials and combinations of nanomaterials as well as deposition on curved surfaces. Such extensions would allow us to create a variety of nanomaterial-based artificial structures, similar to those achieved using semiconductor growth technology. In particular, the demonstration of strong interlayer plasmonic coupling and the possibility of depositing nanoparticle films with a large number of layers open a new route to designer plasmonic metamaterials.

Acknowledgment. The authors thank Prof. Hiroyuki Sugimura (Kyoto University) for supplying the ultrasmooth ITO-coated quartz substrates and Chieh-Lun He and Yun-Tzu Chiu for the synthesis of colloidal Ag nanoparticle solutions. The TEM images shown in Figure S1 in the Supporting Information were acquired by Dr. Chun-Hong Kuo, and the synchrotron X-ray measurement results shown in Figure S2 were performed by Dr. Hong-Mao Lee; we thank them for their assistance. This research was supported by the National Science Council, Taiwan, through the National Nanoscience and Nanotechnology Program (NSC 98-2120-M-007-009).

Supporting Information Available: Additional information on the synthesis of octadecanethiolate-passivated gold and silver nanoparticles, TEM images of as-synthesized colloidal gold and silver nanoparticles (Figure S1), SXR and GISAXS measurement results (Figure S2), optical measurement setup (Figure S3), and LbL-measured UV−vis absorption spectra (Figure S4). This material is available free of charge via the Internet at http://pubs.acs.org.

JA103722P

(36) Schider, G.; Krenn, J. R.; Hohenau, A.; Ditlbacher, H.; Leitner, A.; Aussenegg, F. R.; Schaich, W. L.; Puscasu, I.; Monacelli, B.; Boreman, G. *Phys. Rev. B* **2003**, *68*, 155427.
(37) Imura, K.; Nagahara, T.; Okamoto, H. *J. Chem. Phys.* **2005**, *122*, 154701.
(38) Payne, E. K.; Shuford, K. L.; Park, S.; Schatz, G. C.; Mirkin, C. A. *J. Phys. Chem. B* **2006**, *110*, 2150–2154.
(39) Khlebtsov, B. N.; Khlebtsov, N. G. *J. Phys. Chem. C* **2007**, *111*, 11516–11527.
(40) Okamoto, H.; Imura, K. *Prog. Surf. Sci.* **2009**, *84*, 199–229.
(41) Miyazaki, H. T.; Kurokawa, Y. *Phys. Rev. Lett.* **2006**, *96*, 097401.
(42) Harris, N.; Arnold, M. D.; Blaber, M. G.; Ford, M. J. *J. Phys. Chem. C* **2009**, *113*, 2784–2791.